Fully Tricoordinated Assembly Unveils a Pioneering Nonlinear Optical Crystal $(SbTeO_3)(NO_3)$

Bo Zhang,[a],[b] Chun-Li Hu,[a],[b] Jiang-Gao Mao,[a],[b] and Fang Kong*[a],[b]

[a] State Key Laboratory of Structural Chemistry, Fujian Institute of Research on the Structure of Matter, Chinese Academy of Sciences, Fuzhou 350002, P. R. China

[b] University of Chinese Academy of Sciences, Beijing 100049, P. R. China

*Corresponding Authors: kongfang@fjirsm.ac.cn

Contents

Experimental Section

Reagents

All the chemicals were obtained from commercial sources and used without further purification: $Sr(NO_3)_2$ (Aladdin, 99.90%), TeO_2 (Shanghai Yuya New Material Technology, 99.99%), SbF_3 (Macklin, 99.99%), and HF (Aladdin, 40%). *Caution: hydrofluoric acid is toxic and corrosive! It must be handled with extreme caution and with the appropriate protective equipment and training.*

Syntheses

Single crystalline samples of $(SbTeO_3)(NO_3)$ were successfully synthesized via a solvent volatilization reaction based on the following chemical proportions: SbF_3 (1.0 mmol), TeO_2 (2.0 mmol) and $Sr(NO_3)_2$ (2.0 mmol), hydrofluoric acid (5 drops) and 5 mL of deionized water. The mixture was put into a clean beaker, then place it on a magnetic stirrer and stir for 15 minutes. Afterwards, let it evaporate at room temperature in a fume hood for 6 days. Finally, only a small amount of solvent remains in the beaker. colorless rod-shaped transparent crystals were obtained by washed with deionized water, filtered and dried in air.

Powder X-ray diffraction

Powder X-ray diffffraction (PXRD) data of $(SbTeO_3)(NO_3)$ were collected on the Miniflex 600 powder X-ray diffractometer using Cu Kα radiation (λ = 1.54186 Å) at room temperature in the angular range of 2θ = 5-70° with a scan step size of 0.02°.

Energy-dispersive X-ray spectroscopy

Microprobe elemental analysis was carried out with the aid of a field-emission scanning electron microscope (JSM6700F) outfitted with an energy-dispersive X-ray spectroscope (Oxford INCA).

Spectroscopic measurements

IR spectrum was carried out on a Magna 750 FT-IR spectrometer using air as background in the range of 4000–400 cm^{-1} with a resolution of 2 cm^{-1} at room temperature. The measurement was performed using a UV-vis-NIR spectrophotometer with an integrating sphere attachment. The powder crystals samples were placed in a sample holder and illuminated with a diffuse light source. The UV-vis-NIR spectrum was obtained in the range of 2000–200 nm by a

PerkinElmer Lambda 950 spectrophotometer using $BaSO_4$ as the reference, and the reflection spectrum were converted into an absorption spectrum using the Kubelka-Munk function. Absorption data was calculated from the diffuse reflection data by the Kubelka-Munk function: $\alpha/S = (1-R)^2/2R$, where α and S represent the absorption coefficient and the scattering coefficient, respectively. The band gap value can be given by extrapolating the absorption edge to the baseline in the α/S vs. energy graph.

Thermogravimetric analyses

The thermogravimetric-differential thermal (TG-DTA) analysis were measured by Netzsch STA 499C installation. The samples about 2.0-10.0 mg were placed in alumina crucibles and heated in 20-1200 °C at a rate of 15 °C/min under N_2 atmosphere.

Powder SHG measurements

Powder SHG measurements were conducted using a modified method of Kurtz and Perry. Irradiation laser (λ = 1064 nm) is generated by a Nd:YAG solid-state laser equipped with a Q switch. The $(SbTeO_3)(NO_3)$ pure crystal samples ground into powder were sieved according to seven different particle size ranges (45−53, 53−75, 75−105, 105−150, 150−210 and 210−300 μm). KH_2PO_4 (KDP) samples in the same size range were also be prepared, which were used as reference. SHG signals oscilloscope traces of $Sb(TeO_3)(NO_3)$ and KDP samples in the particle size range (150−210 μm) were recorded.

The LIDT measurements

The LIDT measurements of the $(SbTeO_3)(NO_3)$ crystal samples was performed by a Q-switched pulsed laser. The particle size range of the tested sample was 150−210 μm, the laser wavelength was 1064 nm, the pulse duration was 10 ns, the pulse frequency was 1 Hz, and the laser spot area focused on the sample was 2.54 mm^2. The energy of the laser emission was gradually increased during the measurement, and the LIDT of the sample was determined when it turned black under the laser.

Birefringence Measurements

The birefringence of $(SbTeO_3)(NO_3)$ were measured with a polarizing microscope (ZEISS Axio Scope A1) equipped with the Berek compensator. The small and transparent $(SbTeO_3)(NO_3)$ crystal were chosen for measurement. The thickness of the selected crystal was

measured on the polarizing microscope. The formula for calculating the birefringence is listed below:

$$R = \Delta n \times T$$

where R denotes the optical path difference, Δn represents the birefringence, and T is the thickness of the crystal.

Single-crystal X-ray diffraction

Single crystal X-ray diffraction data were obtained on Agilent Technologies SuperNova dual-wavelength CCD diffractometer with a graphite-monochromated Mo Kα radiation (λ = 0.71073 Å) at room temperature. Data reduction and cell refinement and were performed with CrysAlisPro. The structure was solved by the direct methods and refined by full-matrix least-squares fitting on F^2 using *OLEX2-1.5* crystallographic software package. All atoms were refined with anisotropic thermal parameters. The structural data were also checked by PLATON and no higher symmetry was found. The detailed crystallographic data for the two compounds were given in Table S1. The bond lengths, calculated bond valences and bond angles were listed in Table S3 and Table S4, respectively.

Computational Method

Single-crystal structural data of compounds $(SbTeO_3)(NO_3)$ were used for the theoretical calculations. The electronic structures were performed using a plane-wave basis set and pseudo-potentials within density functional theory (DFT) implemented in the total-energy code CASTEP.[1] For the exchange and correlation functional, we chose Perdew–Burke–Ernzerhof (PBE) in the generalized gradient approximation (GGA).[2] The interactions between the ionic cores and the electrons were described by the ultrasoft pseudopotential.[3] The following valence-electron configurations were considered in the computation: Sb-$5s^25p^3$, Te-$5s^25p^4$, O-$2s^22p^4$ and N-$2s^22p^3$. The numbers of plane waves included in the basis sets were determined by cutoff energy of 750 eV for $(SbTeO_3)(NO_3)$. The numerical integration of the Brillouin zone were 52 performed using Monkhorst-Pack k-point sampling of 3 × 3 × 3. The other parameters and convergent criteria were the default values of CASTEP code.

The calculations of second-order NLO susceptibilities were based on length-gauge formalism within the independent particle approximation.[4, 5] The second-order NLO

susceptibility can be expressed as

$$\chi_{\mathrm{L}}^{abc}(-2\omega;\omega,\omega)=\chi_{\mathrm{inter}}^{abc}(-2\omega;\omega,\omega)+\chi_{\mathrm{intra}}^{abc}(-2\omega;\omega,\omega)+\chi_{\mathrm{mod}}^{abc}(-2\omega;\omega,\omega)$$

where the subscript L denotes the length gauge, $\chi_{\mathrm{inter}}^{abc}$, $\chi_{\mathrm{intra}}^{abc}$ and $\chi_{\mathrm{mod}}^{abc}$ give the contributions to χ_{L}^{abc} from interband processes, intraband processes, and the modulation of interband terms by intraband terms, respectively.

According to sum-over-states formalism, each orbital's contribution to a specific SHG coefficient can be identified. Using the normalized effective SHG of each orbital as a weighting coefficient, and summing all the SHG-weighted orbitals in VB or CB over different k-points in the space, the SHG-weighted electron density ("SHG-density" for short) can be obtained.[6] Through SHG-density plots, the electronic states which give significant contributions to the SHG coefficient can be visualized. The contributed values of groups to the SHG coefficient can also be calculated. First, the electron density of the compound is cut in the real space, concretely, the electron density of each grid point is assigned to the corresponding atom by using kinds of cutting methods, e.g. gradient path interpolation tracing (GPIT) method, etc. Then based on the SHG-density data, the SHG values of all the grid points belonging to a certain atom are summed up to obtain the SHG contribution value of the atom. Finally, the SHG contribution of a group can be further obtained by summing up those of all atoms in the group.

The calculations of linear optical properties in terms of the complex dielectric function $\varepsilon(\omega)=\varepsilon_1(\omega)+i\varepsilon_2(\omega)$ were made. The imaginary part of the dielectric function ε_2 was given in the following equation:

$$\varepsilon_2^{ij}(\omega)=\frac{8\pi^2\hbar^2e^2}{m^2V}\sum_k\sum_{cv}(f_c-f_v)\frac{p_{cv}^i(k)p_{vc}^j(k)}{E_{vc}^2}\delta[E_c(k)-E_v(k)-\hbar\omega]$$

The f_c and f_v represent the Fermi distribution functions of the conduction and valence band. The term $p^i_{cv}(k)$ denotes the momentum matrix element transition from the energy level c of the conduction band to the level v of the valence band at the kth point in the Brillouin zone (BZ) (Table S7), and V is the volume of the unit cell.

The real part $\varepsilon_1(\omega)$ of the dielectric function $\varepsilon(\omega)$ follows from the Kramer–Kronig relationship. All the other optical constants may be derived from $\varepsilon_1(\omega)$ and $\varepsilon_2(\omega)$. For example, the refractive index $n(\omega)$ can be calculated using the following expression[7]:

$$n(\omega)=\left(\frac{1}{\sqrt{2}}\right)\left[\sqrt{\varepsilon_1^2(\omega) + \varepsilon_2^2(\omega)} + \varepsilon_1(\omega)\right]^{1/2}$$

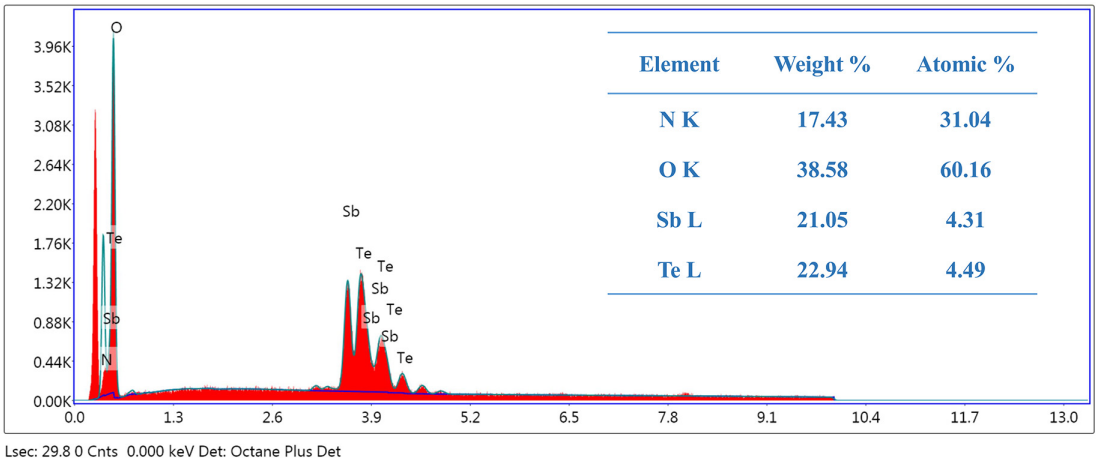

Element	Weight %	Atomic %
N K	17.43	31.04
O K	38.58	60.16
Sb L	21.05	4.31
Te L	22.94	4.49

Figure S1. The energy-dispersive X-ray spectroscopy for $(SbTeO_3)(NO_3)$

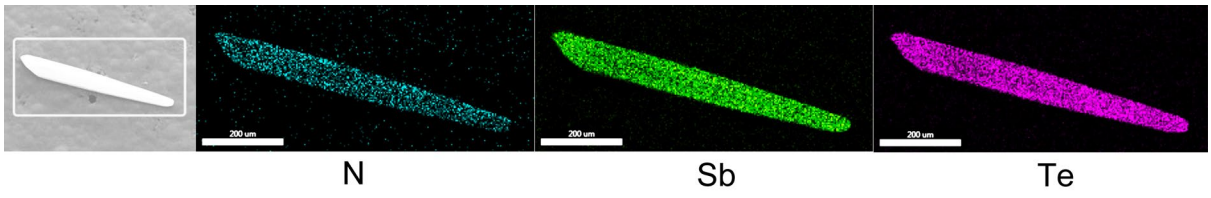

Figure S2. SEM images of $(SbTeO_3)(NO_3)$ and its elemental distribution maps.

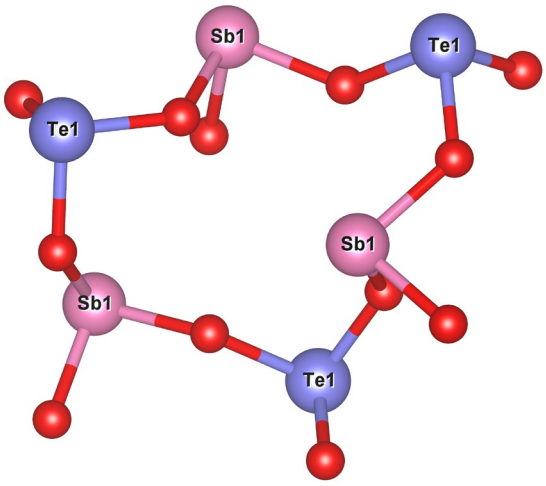

Figure S3. The $[Sb_3Te_3]$ 6-member polyhedral rings (MPRs) in $[SbTeO_3]^+$ cationic layer.

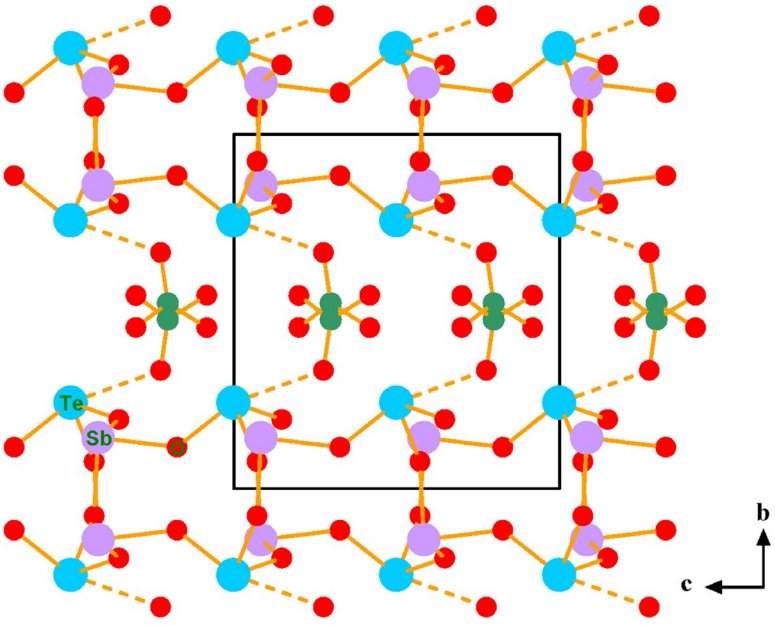

Figure S4. The 3D structure of $(SbTeO_3)(NO_3)$ connected by weak Te-O bonds.

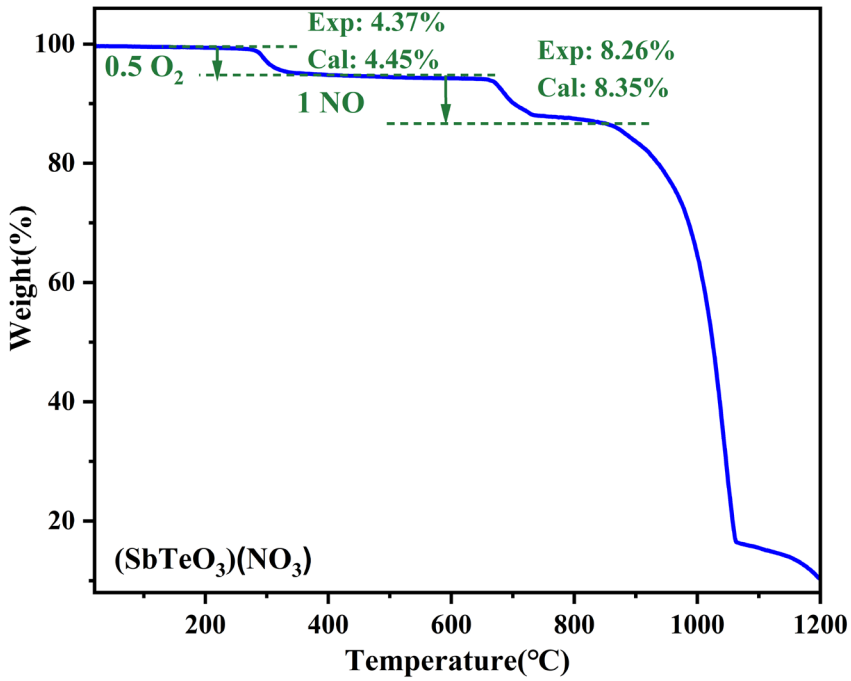

Figure S5. Thermogravimetric analysis (TGA) of $(SbTeO_3)(NO_3)$ under N_2 atmosphere.

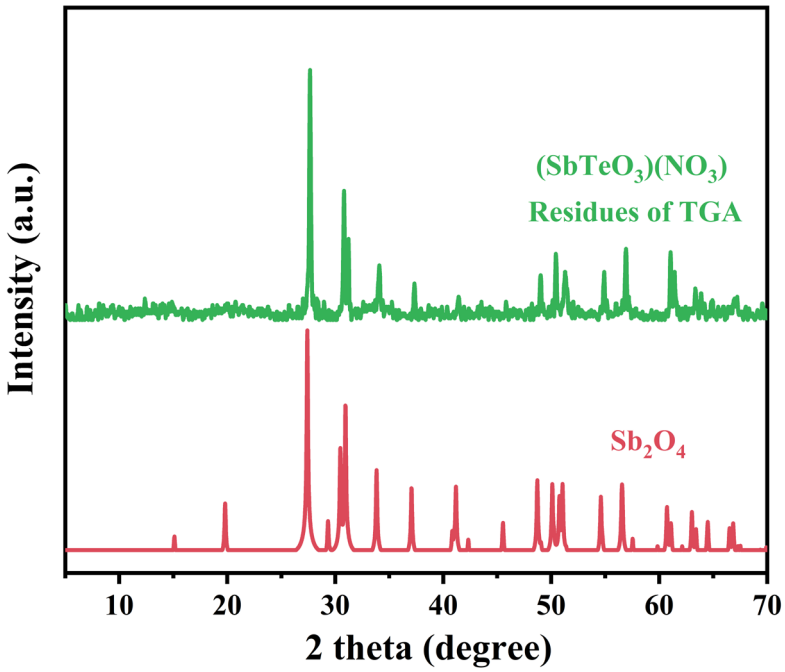

Figure S6. PXRD patterns of Sb_2O_4 and the residue of $(SbTeO_3)(NO_3)$ after 1000 °C.

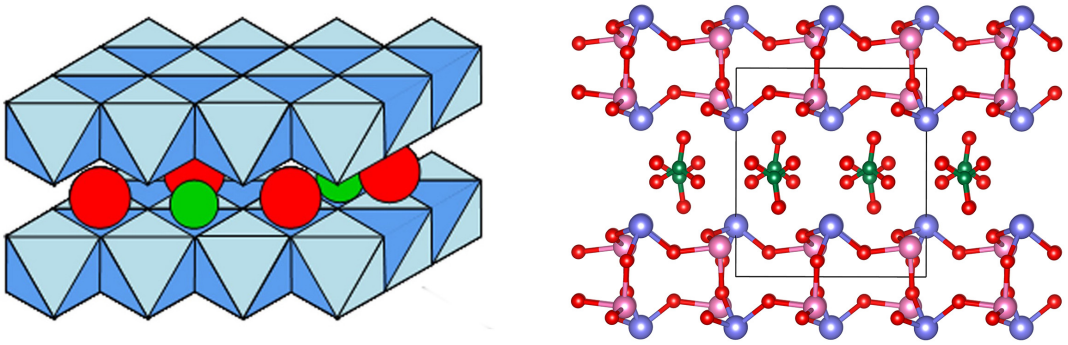

Layered double hydroxides **$(SbTeO_3)(NO_3)$**

Figure S7. The structural comparison between layered double hydroxides (LDHs) and $(SbTeO_3)(NO_3)$.

Table S1. Crystal data and structure refinement for $(SbTeO_3)(NO_3)$.

molecular formula	$(SbTeO_3)(NO_3)$
Formula Weight	359.36
crystal system	orthorhombic
space group	$Pca2_1$
Temperature(K)	99.99(10)
F(000)	632.0
a/Å	7.5924(2)
b/Å	8.6596(3)
c/Å	7.9492(3)
α(deg)	90
β(deg)	90
γ(deg)	90
V/Å^3	522.64(3)
Z	4
Dc(g.cm^{-3})	4.567
GOF on F^2	1.081
Flack factor	-0.01(4)
R1, wR2[I > 2σ(I)]α	0.0166, 0.0364
R1, wR2 (all data)α	0.0170, 0.0366

$^{\alpha}$ $R_1 = \sum||F_o| - |F_c||/\sum|F_o|$, $wR_2 = \{\sum w[(F_o)^2 - (F_c)^2]^2/\sum w[(F_o)^2]^2\}^{1/2}$

Table S2. Fractional atomic coordinates ($\times 10^4$) and equivalent isotropic displacement parameters ($Å^2 \times 10^3$) for $(SbTeO_3)(NO_3)$. U_{eq} is defined as 1/3 of the trace of the orthogonalised U_{ij} tensor.

	Atom	x	y	z	U(eq)
$Sb(TeO_3)(NO_3)$	Sb(1)	6085.3(4)	1437.1(4)	9166.5(7)	5.51(12)
	Te(1)	4590.7(4)	2429.8(4)	5012.2(7)	5.14(11)
	N(1)	3556(6)	4770(6)	2025(7)	8.8(11)
	O(1)	2867(5)	5457(5)	829(6)	11.7(10)
	O(2)	4600(5)	5450(5)	3003(6)	10.1(9)
	O(3)	3240(6)	3338(5)	2249(6)	10.0(10)
	O(4)	6448(5)	1956(6)	3526(6)	7.8(9)
	O(5)	3144(5)	767(4)	4287(7)	7.2(8)
	O(6)	5621(6)	1170(5)	6742(6)	7.4(9)

Table S3. The bond lengths (Å) and calculated bond valences for $(SbTeO_3)(NO_3)$.

Compound	Bond	Bond-length	Bond-valence	BVS
$Sb(TeO_3)(NO_3)$	Sb(1)-O(4)#1	1.992(4)	0.949	2.879
	Sb(1)-O(5)#2	1.999(4)	0.931	
	Sb(1)-O(6)	1.973(5)	0.999	
	Te(1)-O(4)	1.885(4)	1.281	3.667
	Te(1)-O(5)	1.901(4)	1.227	
	Te(1)-O(6)	1.922(4)	1.159	
	N(1)-O(1)	1.238(7)	1.686	4.818
	N(1)-O(2)	1.256(7)	1.606	
	N(1)-O(3)	1.275(7)	1.526	

Symmetry transformations used to generate equivalent atoms: #1 3/2-X, +Y, 1/2+Z; #2 1-X, -Y, 1/2+Z

Table S4. The bond angles (deg.) for $(SbTeO_3)(NO_3)$.

$(SbTeO_3)(NO_3)$			
O(4)-Sb(1)-O(5)#2	87.26(18)	O(5)-Te(1)-O(6)	91.3(2)
O(6)-Sb(1)-O(4)#1	86.82(18)	O(1)-N(1)-O(2)	121.1(5)
O(6)-Sb(1)-O(5)#2	89.3(2)	O(1)-N(1)-O(3)	119.7(5)
O(4)#3-Te(1)-O(5)	94.4(2)	O(2)-N(1)-O(3)	119.2(5)
O(4)-Te(1)-O(6)	91.2(2)		

Symmetry transformations used to generate equivalent atoms: #1 3/2-X, +Y, 1/2+Z; #2 1-X, -Y, 1/2+Z

Table S5. The dipole moments of the polar units in $(SbTeO_3)(NO_3)$ and their net dipole moments in a unit cell (D = Debyes).

$(SbTeO_3)(NO_3)$				
Polar unit	Dipole moment (D)			
	total magnitude	x-component	y-component	z-component
TeO_3	6.884	(±4.045)+(±4.047)	(±10.649)+(±10.651)	(-1.721)×4
SbO_3	28.84	(±6.234)×2	(±5.012)×2	(-7.210)×4
NO_3	0.548	(±0.415)×2	(±0.560)×2	(-0.137)×4
Net dipole moment (a unit cell)	36.272	0	0	-36.272

Table S6. A summary of reported tellurite nitrates, antimony nitrates and antimony tellurites families.

Compound	Number	Space Group	SHG Intensity	Eg (eV)	PM	Reference
Te(IV)-NO_3						
$Bi_3(OH)(TeO_3)_3(NO_3)_2$	1	*P*-62*m*	0.5×KDP	3.31	/	[8]
$Bi_2Te_2O_6(NO_3)_2(OH)_2(H_2O)$	2	$P2_12_12_1$	20×α-SiO_2	4.0	YES	[9]

$[Bi(TeO_3)](NO_3)$	3	$P2_1/c$	/	3.62	/	[10]
$La(TeO_3)(NO_3)$	4	$P2_1/n$	/	3.7	/	[11]
$Nd(TeO_3)(NO_3)$	5	$P2_1/n$	/	3.6	/	[11]
$Eu(TeO_3)(NO_3)$	6	*Cmca*	/	3.7	/	[11]
$Gd(TeO_3)(NO_3)$	7	*Cmca*	/	3.8	/	[11]
$Dy(TeO_3)(NO_3)$	8	*Cmca*	/	3.8	/	[11]
$Er(TeO_3)(NO_3)$	9	*Cmca*	/	3.8	/	[11]
$Y(TeO_3)(NO_3)$	10	*Cmca*	/	4.4	/	[11]
Sb(III)-NO_3						
$RbSnF_3NO_3$	11	*C2/m*	/	3.69	/	[12]
$Rb_2SbF_3(NO_3)_2$	12	$P2_1$	2.7×KDP	3.76	YES	[12]
$Rb_3SbF_3(NO_3)_3$	13	$P2_1$	2.2×KDP	3.75	YES	[13]
$(NH_4)_3SbF_3(NO_3)_3$	14	$P2_1$	3.3×KDP	3.77	YES	[14]
$(NH_4)_3SbF_4(NO_3)_2$	15	*Pnma*	/	3.64	/	[14]
Sb(III)-Te(IV)						
$SbTeO_3Cl$	16	*Pnma*	/	3.81	/	[15]
$SbTeO_3Br$	17	*Pnma*	/	3.64	/	[15]
$[Sb_2(TeO_4)](SO_4)$	18	*P*-1	/	4.16	/	[16]
$[Sb_2(TeO_3)_2](SO_4)$	19	*Pbca*	/	3.72	/	[16]
$Sb_4O_3(TeO_3)_2(HSO_4)(OH)$	20	*C2/c*	/	3.65	/	[17]
$(SbTeO_3)(NO_3)$	/	$Pca2_1$	2.2×KDP	4.32	YES	This work

Table S7. State energies (eV) of the highest valence band (H-VB) and the lowest conduction band (L-CB) of $(SbTeO_3)(NO_3)$.

Compound	K-point	H-VB	L-CB
$(SbTeO_3)(NO_3)$	G(0.000, 0.000, 0.000)	-0.1312	3.38936
	Z(0.000, 0.000, 0.500)	-0.11987	2.42445
	T(-0.500, 0.000, 0.500)	-0.18119	3.49746
	Y(-0.500, 0.000, 0.000)	-0.16089	3.37245
	S(-0.500, 0.500, 0.000)	-0.09733	3.32714
	X(0.000, 0.500, 0.000)	0	3.35007
	U(0.000, 0.500, 0.500)	-0.12961	3.47287
	R(-0.500, 0.500, 0.500)	-0.17999	3.5339

References

1. M. D. Segall, P. J. D. Lindan, M. J. Probert, C. J. Pickard, P. J. Hasnip, S. J. Clark and M. C. Payne, *J. Phys.: Condens. Matter*, 2002, **14**, 2717–2744.
2. V. Milman, B. Winkler, J. A. White, C. J. Pickard, M. C. Payne, E. V. Akhmatskaya and R. H. Nobes, *Int. J. Quantum Chem.*, 2000, **77**, 895-910.
3. J. P. Perdew, K. Burke and M. Ernzerhof, *Phys. Rev. Lett.*, 1996, **77**, 3865–3868.
4. S. Sharma, J. K. Dewhurst and C. Ambrosch-Draxl, *Phys. Rev. B*, 2003, **67**, 165332.
5. J. E. Sipe and E. Ghahramani, *Phys. Rev. B*, 1993, **48**, 11705-11722.
6. C. H. Lo and M. H. Lee, Master Thesis, Tamkang University, 2005.
7. D. Vanderbilt, *Phys. Rev. B*, 1990, **41**, 7892-7895.
8. J. L. Song and C. Qian, *ChemistrySelect*, 2017, **2**, 1681–1685.
9. S. Lee, H. Jo and K. M. Ok, *J. Solid State Chem.*, 2019, **271**, 298–302.
10. C. Y. Meng, M. F. Wei, L. Geng, P. Q. Hu, M. X. Yu and W. D. Cheng, *J. Solid State Chem.*, 2016, **239**, 46–52.
11. H. E. Lee, H. Jo, M. H. Lee and K. M. Ok, *J. Alloys Compd.*, 2021, **851**, 156855.
12. L. Wang, H. m. Wang, D. Zhang, D. J. Gao, J. Bi, L. Huang and G. h. Zou, *Inorg. Chem. Front.*, 2021, **8**, 3317–3324.
13. L. Wang, F. Yang, X. Y. Zhao, L. Huang, D. J. Gao, J. Bi, X. Wang and G. H. Zou, *Dalton Trans.*, 2019, **48**, 15144–15150.
14. Q. Wang, J. X. Ren, D. Wang, L. L. Cao, X. H. Dong, L. Huang, D. J. Gao and G. H. Zou, *Inorg. Chem. Front.*, 2023, **10**, 2107–2114.
15. X. Y. Zhou, X. Mao, P. Zhang, X. H. Dong, L. Huang, L. L. Cao, D. J. Gao and G. H. Zou, *Inorg. Chem. Front.*, 2024, **11**, 3221–3228.
16. J. Y. Zhang, X. Zhao, Y. D. Wu, D. J. Mei, S. G. Wen and T. Doert, *Z. Anorg. Allg. Chem.*, 2021, **647**, 1269–1276.
17. X. F. Li, K. Wang, C. He, J. H. Li, X. T. An, J. Pan, Q. Wei, G. M. Wang and G. Y. Yang, *Inorg. Chem.*, 2023, **62**, 7123–7129.